Temperature dependence and activation energy of electrical conduction in an engineered cementitious composite

PAPER • **OPEN ACCESS**

Temperature dependence and activation energy of electrical conduction in an engineered cementitious composite

To cite this article: B Suryanto *et al* 2020 *IOP Conf. Ser.: Mater. Sci. Eng.* **930** 012053

IOP Conf. Series: Materials Science and Engineering **930** (2020) 012053 doi:10.1088/1757-899X/930/1/012053

Temperature dependence and activation energy of electrical conduction in an engineered cementitious composite

B Suryanto[1]*, D Saraireh[1] and A Tambusay[1,2]

[1] Institute for Infrastructure and Environment, School of Energy, Geoscience, Infrastructure and Society, Heriot-Watt University, Edinburgh, United Kingdom.
[2] Department of Civil Engineering, Faculty of Civil, Planning and Geo Engineering, Sepuluh Nopember Institute of Technology, Surabaya, East Java, Indonesia.

*Corresponding author's e-mail: B.Suryanto@hw.ac.uk

Abstract. The electrical impedance of an engineered cementitious composite was measured over the temperature range 7–60°C and data are presented over the frequency range 20Hz–1MHz. The work has highlighted that the resistive and reactive components of the complex impedance both displayed an inverse relationship with temperature. When presented in an Arrhenius format, the bulk resistance displayed a linear response over the entire temperature range studied and the activation energy, E_a, for electrical conduction was evaluated as 21.7 kJ/mol (0.22 eV/ion).

1. Introduction

Engineered Cementitious Composite (ECC) is a family of cement composite that is capable of exhibiting strain hardening response in tension, with a tensile strain capacity in the order of a few percent commonly achieved [1]. This unique property is attributed to the ability of this group of cement composite to form multiple micro-cracks of small widths (typically <0.1 mm) [2, 3], thereby making it particularly attractive for applications where cracking and long-term durability are critical. Two areas of application that have received increasing attention are durable cover and repair material [4, 5]; therefore, it is not surprising that the durability and long-term performance of ECC in the natural environment have been actively researched by various laboratories around the world [6-9].

Recently, there has been a growing interest in exploiting the self-monitoring capabilities of ECC, through monitoring of its electrical properties [10-12]. Due to the vagaries of weather in the natural environment, however, ECC will certainly be subjected to constantly changing load and environmental (i.e. temperature and humidity) conditions which would, in turn, affect its electrical response. The latter is particularly relevant for ECC applied in the near-surface region, as if used as a cover or repair material. As far as electrical based monitoring is concerned, there is a need to develop a systematic approach that can be used to treat the effects of every contributing factor on electrical response (i.e. temperature, moisture, cracking/damage) in isolation. It is set against this background that this paper presents the findings of a testing programme that investigates the influence of temperature on bulk electrical properties. Data are presented in the Arrhenius format, thereby allowing evaluation of the activation energy for electrical conduction. The knowledge gained from this work will be used for developing an activation energy-based temperature correction protocol which can be used to remove temperature effects from field measurements.

2. Experimental Programme

2.1. Materials and mix proportion

The mix proportion for the ECC used in this experimental programme is presented in table 1. The binder comprised Portland cement CEM I 52.5N to BS EN197-1 [13] and fine fly-ash (Superpozz SV80, supplied by ScotAsh) at a cement/fly-ash ratio of 1:1.8 (or a replacement level of approximately 64%). The typical oxide analysis of these materials is presented in table 2. Fine silica sand with a mean particle size of 120 μm was added into the mix at a sand/cement ratio of 0.6:1 by mass. The fibres used in the mix were Kuralon K-II REC15 polyvinyl alcohol fibres, which were added at a dosage of 2% by volume. The fibres had an average diameter of 39 μm, length of 12mm, tensile strength of 1.6GPa, and tensile strain capacity of 6.5%. They were supplied with a proprietary coating agent (1.2% by mass) by the manufacturer to reduce excessive chemical bonding with the surrounding matrix. A high-range water-reducing (HRWR) admixture (BASF MasterGlenium ACE499) was added at a dosage rate of 1% by mass of binder to improve mix workability and fibre dispersion. The water/binder ratio was set at a relatively low value (=0.28) to produce an ECC matrix of desired strength.

Table 1. Summary of ECC mix and compressive strengths.

OPC (kg/m^3)	FA (kg/m^3)	S (kg/m^3)	HRWR (kg/m^3)	PVA (kg/m^3)	w/b	Compressive strength (MPa)		
						28 days	90 days	180 days
454	818	273	4.54	2.6	0.28	51.9	63.7	66.6

Notes: OPC: CEM I 52.5N; FA: fly ash; S: sand; HRWR: high-range water-reducing admixture; and PVA: polyvinyl alcohol.

Table 2. Typical oxide analysis of materials (+ = not determined).

Properties	OPC	FA
Chemical analysis		
SiO_2	19.9	52.7
Al_2O_3	4.8	26.6
Fe_2O_3	3.1	5.6
K_2O	+	+
CaO	62.4	2.4
MgO	2.2	1.2
Na_2O equivalent	0.54	1.7
SO_3	3.0	0.3
Free CaO	+	0.03
Total phosphate	+	0.5
Loss on Ignition (LOI)	+	<2.0
Physical properties		
Specific gravity	3.15	2.20
Surface area (m^2/kg)	375	1300
Fineness (% retained on 25 μm)	+	<25

2.2. Test specimens, fabrication and curing

In this experimental programme, a total of 14 ECC specimens were fabricated. As illustrated in figure 1, three, 40×40×160 (long) mm prismatic specimens were used for electrical measurements (see figure 1(a)); five, dog-bone (DB) shaped specimens of geometry and dimensions in accordance with the JSCE recommendation [14] for tensile testing (see figure 1(b)); and six, 50 mm cuboidal specimens for compressive strength tests.

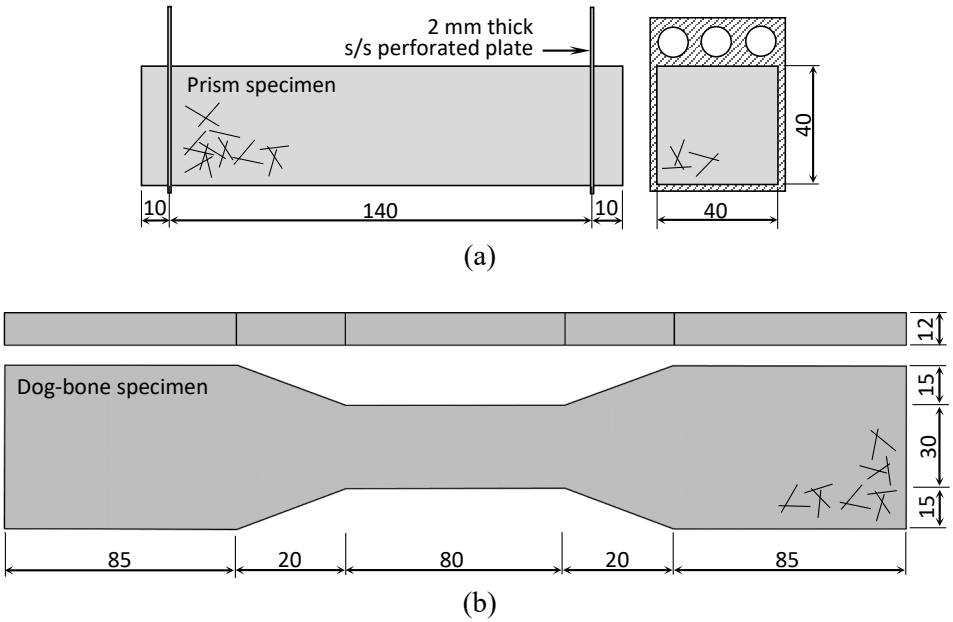

Figure 1. Schematic of test specimens: (a) prism; and (b) dog-bone shaped (DB) specimen. All dimensions are in mm.

A 10-litre Hobart planetary motion mixer was used to prepare the mix in a single batch. Specimens for electrical measurements were cast in polystyrene moulds, with a pair of 45×65×2 (thick) mm stainless steel (316L) perforated electrodes provided at the time of casting at 140 mm ceantres to facilitate electrical measurements. The perforations on the electraodes were 10 mm in diameter and arranged in a staggered pattern with a 15 mm pitch. The relatively large hole size was chosen to allow for the ECC slurry to flow easily through the perforations during casting. The use of perforated electrodes also ensured intimate bonding with the ECC and reduced any possible interfacial problem at the electrode/sample contact region [15]. The dog bone and cube specimens were cast in custom-made Plexiglas and standard three-gang steel moulds, respectively. All these moulds were treated with a proprietary release agent prior to casting.

After casting, all specimens were covered with thick cling film and allowed to cure for 24 hours. The specimens were then demoulded and stored in a curing tank at 20±2°C until they were required for testing (28 days for the dog-bone specimens; 28, 90 and 180 days for the cubes; and 360 days for the prisms). With regard to the latter, hydration could be considered as having ceased and, as such, at this extended period of time, the electrical response would be purely due to the changing in temperature.

2.3. Specimen conditioning and electrical measurements

Prior to testing, each prism specimen was removed from the curing tank and then placed in a thermostatically controlled circulating water bath (initially at ≈7ºC). The water was then raised to the temperature at which electrical measurements were required, which, in the case of the work presented, at 10 to 60ºC in 10ºC increments (with one additional measurement at 15ºC). At the required temperature, temperature was held for ~5 minutes in order to minimise thermal gradient within the specimen. This was confirmed by monitoring the internal temperature within each specimen (through a thermistor which was embedded at the time of casting). Once thermal equilibrium was reached, electrical impedance measurement was then undertaken on each specimen using an E4980AL Keysight high-precision LCR meter. The LCR meter was operated at a constant signal amplitude of 350mV and controlled by a desktop PC using LabVIEW virtual instrument. A logarithmic sweep was made over the frequency range 20Hz–1MHz, with the impedance recorded at 20 spot frequencies within this range. The connection to the LCR meter was by means of four individually-screened (short) coaxial cables, with connection to the electrode by means of alligator clips.

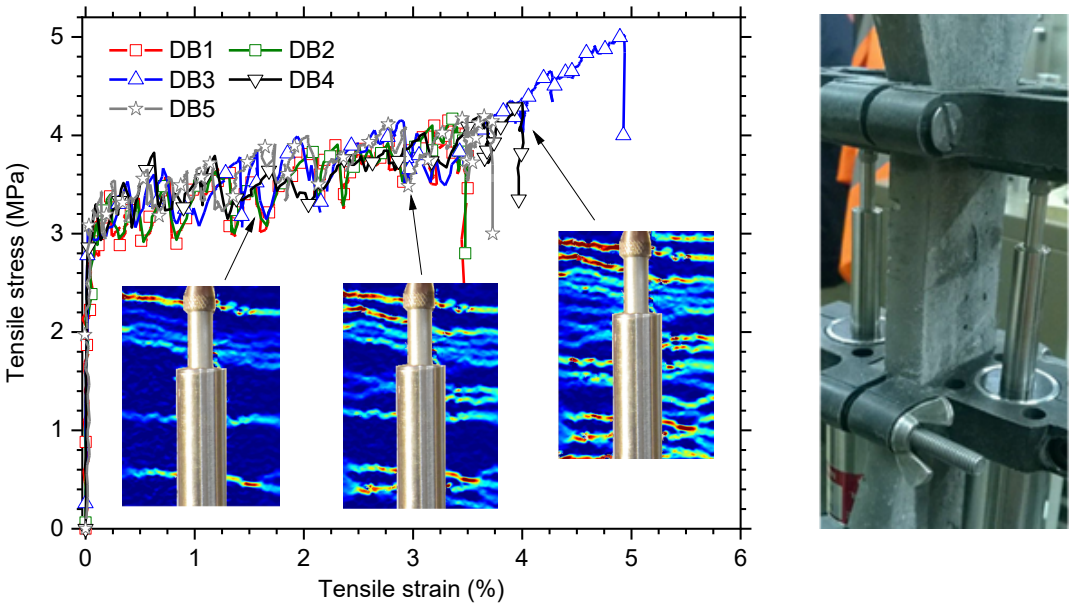

Figure 2. (a) Typical tensile stress-strain response obtained from dog-bone specimens; and (b) specimen during tensile testing showing two displacement transducers for strain measurements.

Although the focus of this paper is on the electrical properties of an ECC, it was considered appropriate to confirm the tensile strain hardening properties of the material and, for completeness, check the strength development with time. The dog-bone specimens were therefore tested using a 100kN 4206 Instron at 28 days after casting. Each specimen was held at both ends using pneumatic grips and loading was then applied under a crosshead speed of 0.5 mm/min. Figure 2(a) presents the tensile stress-strain responses obtained from the dog-bone specimens, together with an example of the crack patterns obtained using an automated crack mapping technique [16, 17]. It is evident that all specimens displayed a tensile strain hardening response with notable fluctuations in stress with increasing strain, highlighting clearly its distinctive tensile strain-hardening property. The fluctuations in stress can be attributed mainly to progressive development of micro-cracks and the evidence for this can be seen from the strain plots displayed in the figure, which were obtained from the central (narrower) section of the dog-bone. The strength development of the ECC over a 180-day period was determined by testing the ECC cubes using a 3000kN Avery-Denison testing machine, with the load applied at a rate of 50kN/min. The compressive strengths obtained on the 28th, 90th and 180th days of curing are presented in table 1.

2.4. Preliminaries and data presentation

The impedance, $Z(\omega)$, of a cementitious system (in Ohm, Ω) subjected to a small-signal sinusoidal electric field at an angular frequency, ω, can be written in rectangular form as,

$$Q(\omega) = Z'(\omega) - iZ''(\omega) \quad (1)$$

where the real component, $Z'(\omega)$, is the resistive component and the imaginary component, $Z''(\omega)$, is the reactive component (both in Ω). These two parameters are commonly presented in the Nyquist format, with $Z''(\omega)$ plotted against $Z'(\omega)$ over a wide frequency range (see, for example, [18]). For clarity, a typical impedance response obtained using the two-point electrode configuration is presented in figure 3. Two distinct regions are evident: a spur at the right-hand side and a semi-circular arc whose centre is depressed below the real axis at the left-hand side. The intercept of the low-frequency end of the arc with the real axis (i.e. near or at the junction between the electrode spur and the arc, or commonly referred to as the *cusp* point) is easily identifiable and could be considered as the bulk resistance of the test specimen, R (Ω), and will be related to ionic conduction processes [19].

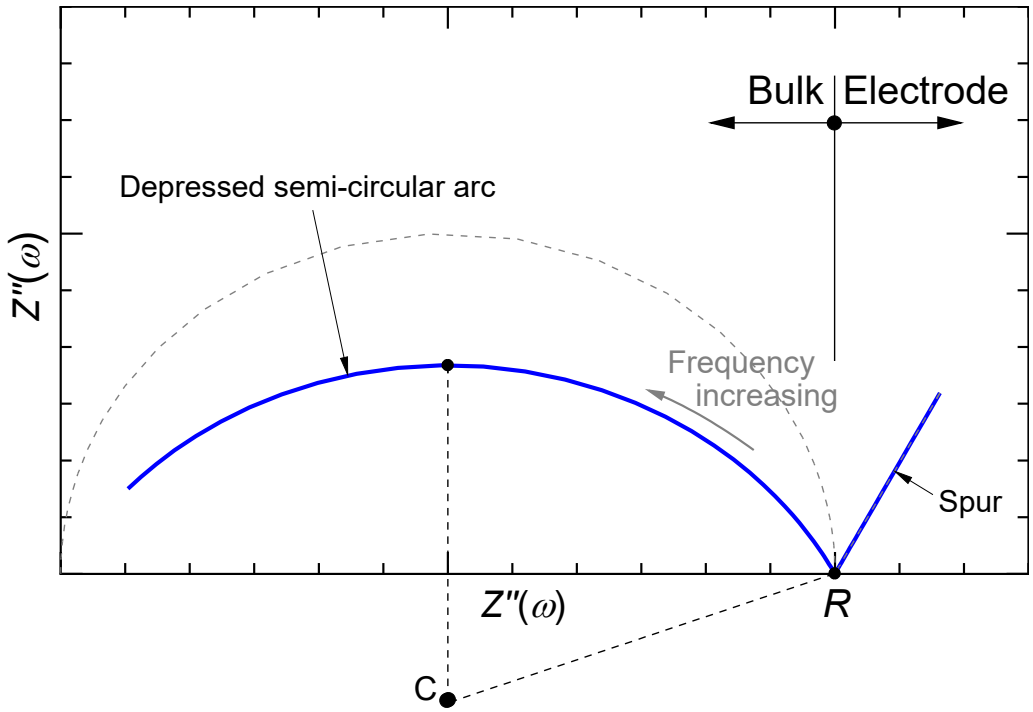

Figure 3. Schematic diagram of the complex impedance response of a cement-based material.

3. Results and Discussion

3.1. Complex impedance and bulk resistance

The typical complex impedance spectra under varying temperatures are displayed in Nyquist format in figure 4(a), with frequency increasing from right-to-left across the curve over the frequency range 20Hz–1MHz. Although measurements were obtained at 20 spot frequencies per decade, for clarity, only selected frequencies are highlighted with data markers. In general terms, a similar overall response to the schematic shown earlier in figure 3 is evident, comprising a depressed semi-circular arc and a weakly developed spur at the low-frequency end; the full extent of the spur would only become apparent at frequencies considerably smaller than the lower frequency limit considered in this study (i.e. << 20 Hz) [20]. The data clearly show that the real and imaginary components of the impedance are both affected by temperature at all test frequencies. As the specimen temperature increases, there is a progressive displacement of the entire impedance response to the left-hand side toward the origin, together with a reduction in the radius of the bulk arc which indicates an overall reduction in specimen impedance. Increasing the specimen temperature has also the effect of shortening the length of the bulk arc, with the end of the arc shifting toward the cusp-point.

Taking the cusp-point as the bulk resistance of the ECC specimen, figure 4(b) displays the variation in resistance as the sample temperature is increased from approximately 7°C to 60°C. Best-fit line to the test data is plotted in the figure in solid line through the measurement points, with the resulting fitting equation displayed on the figure. The results obtained from the two prismatic specimens indicate good repeatability and it is evident that over the temperature range considered, the bulk resistance exhibits an inverse relationship with temperature, with resistance decreasing with increasing temperature, although the changes in resistance at higher temperatures are not as sensitive to changes in temperature as those at lower temperatures. This natural temperature dependence is well-documented and could be attributed primarily to the changes in ionic mobility within the pore network (hence changes in pore-fluid resistance) [21]. In this work, it is anticipated that the influence of other factors such as dissolution of ions and microstructural changes [22] is much limited in extent.

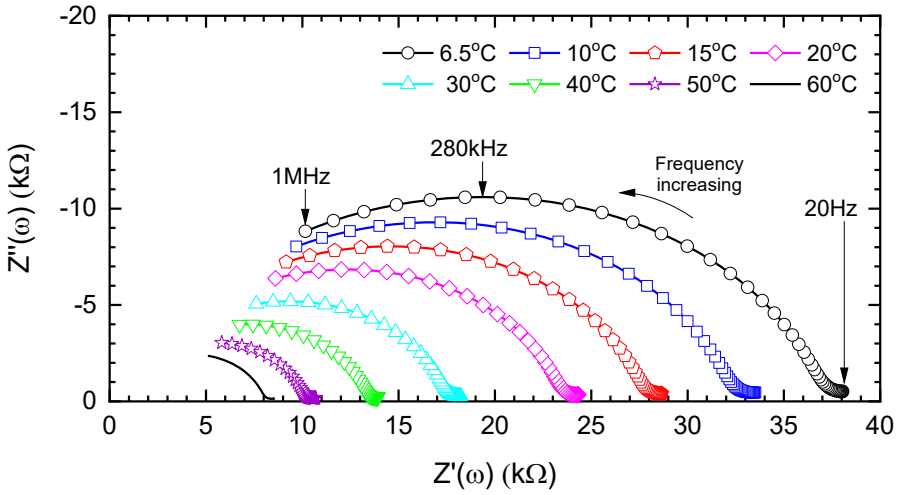

(a)

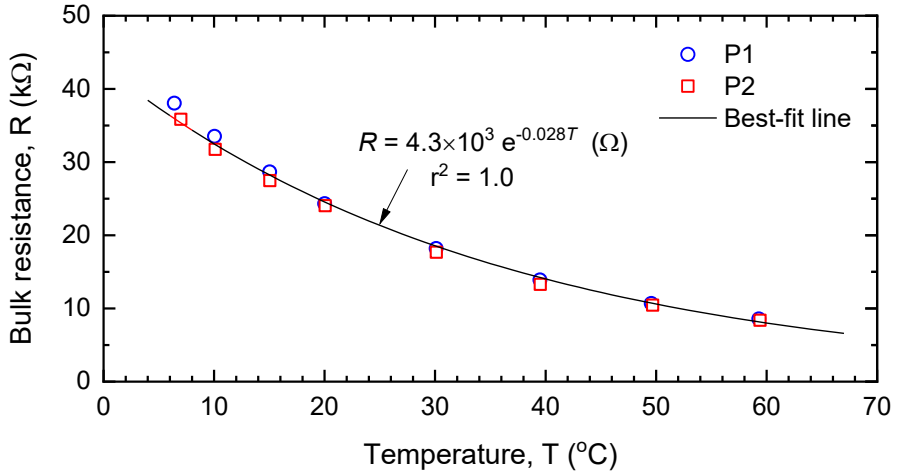

(b)

Figure 4. Variations in (a) impedance and (b) resistance with temperature.

3.2. Arrhenius presentation

Given that ionic conduction in ECC is a thermally activated process, the Arrhenius relationship is applied [22, 23],

$$R = R_o e^{\left[\frac{E_g}{R_g T_k}\right]} \tag{2}$$

where R is the bulk resistance (Ω) at temperature T_k (Kelvin); R_o is the pre-exponential constant and represents the nominal resistance at infinite temperature (Ω); E_a is the activation energy for the conduction process (J mol^{-1}); R_g is Universal Gas constant (8.3141 J mol^{-1} K^{-1}). Figure 5 presents the natural logarithm of bulk resistance, $ln(R)$, plotted against $1000/T_k$. In this format of presentation, the sample temperature increases from right-to-left along the horizontal axis; the data markers represent the measured resistance, while the solid line represents the linear fit from which the slope could be used to obtain the apparent activation energy (i.e. multiplying the slope by R_g will obtain E_a in kJ mol^{-1}). From the data presented, the activation energy for conduction processes over the temperature range 7–60°C was obtained as 21.7 kJ mol^{-1} (0.22 eV per ion) which is in agreement with the value reported in [24].

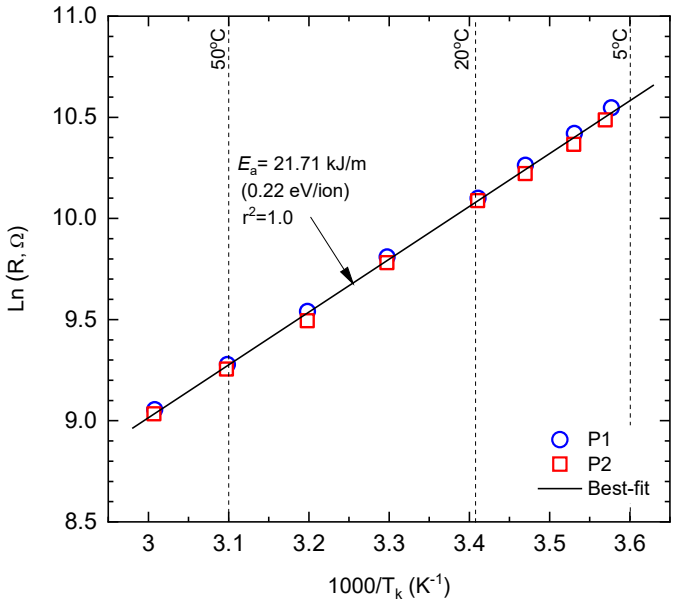

Figure 5. Data in figure 4(b) plotted in Arrhenius format.

Published data on the activation energy for electrical conduction in engineered cementitious composite are very limited; comparisons are, therefore, made with test data obtained from plain Portland cement mortar (water/cement ratio = 0.45), which was evaluated as 19.4 kJ/mol over the range 10–50ºC [21], and Portland cement mortars containing various supplementary cementitious materials (with a constant water/binder ratio = 0.55), which were reported in the range 16–30 kJ/mol [22]. The activation energy obtained in this study could therefore be considered to lie within the range of the anticipated values.

4. Concluding remarks

An Arrhenius plot was established for the conduction process in an engineered cementitious composite, which represents an unresearched area in relation to the electrical response of cementitious systems that are reinforced with polymeric fibres and capable of exhibiting strain-hardening response in tension. Data are presented for ECC specimens undergoing continuous moist curing and, as such, results are directly relevant to ECC that remains saturated. It is shown that an Arrhenius relationship between temperature and bulk resistance does exist, highlighting the fact that electrical conduction in ECC involves a thermally activated process, as typically observed in other cementitious systems. As the self-monitoring version of ECC is now being developed and trialled in the field environment, the knowledge of activation energy will have direct practical significance (i.e. for removing the effect of natural temperature fluctuations) and work is continuing in this respect.

Acknowledgements

The Authors wish to acknowledge the financial support of the Engineering and Physical Sciences Research Council, United Kingdom (Grant EP/N028597/1), Kuraray Japan and GmbH for supplies of PVA fibres, and BASF UK for supplies of water reducers. DS also acknowledges the financial support provided by Heriot-Watt University. Thanks also go to Dr J Kim for assistance in the experimental work.

References

[1] Li V C 2008 Engineered cementitious composites (ECC)–material, structural, and durability performance *Concrete Construction Engineering Handbook* ed E G Nawy (Michigan: CRC Press) chapter 24 pp 1–48

[2] Kanda T, Tomoe S, Nagai S, Maruta M, Kanakubo T and Shimizu K 2006 Full scale processing investigation for ECC precast structural element *J. Asian Archit. Build. Eng.* **5** 2 333–40
[3] Liu H, Zhang Q, Gu C, Su H and Li V C 2016 Influence of micro-cracking on the permeability of engineered cementitious composites *Cem. Concr. Compos.* **72** 104–13.
[4] Kunieda M and Rokugo K 2006 Recent progress on HPFRCC in Japan *J. Adv. Concr. Tech.* **4** 1 19–33
[5] Lepech M D and Li V C 2006 Long term durability performance of engineered cementitious composite *Res. Build. Monum.* **12** 2 119–32
[6] Herbert E N and Li V C 2013 Self-healing of microcracks in engineered cementitious composites (ECC) under a natural environment *Materials* **6** 7 2831–45
[7] Yang E H, Li V C and Qiu J 2015 Early age cracking in a SHCC bridge deck link slab. *7th Congress on Forensic Engineering* (Reston: ASCE) pp 746-55.
[8] Suryanto B, Wilson S A, McCarter W J and Chrisp T M 2016 Self-healing performance of engineered cementitious composites under natural environmental exposure *Adv. Cem. Res.* **28** 4 211–20
[9] Rokugo K 2017 Applications of SHCC in Japan–tools and tips for promoting its use. *Proc. Int. Conf. on Strain-Hardening Cement-Based Composites* (Dordrecht: Springer) pp 671-80
[10] Ranade R, Zhang J, Lynch J P and Li V C 2014 Influence of micro-cracking on the composite resistivity of engineered cementitious composites *Cem. Concr. Res.* **58** 1–12
[11] Suryanto B, McCarter W J, Starrs G, Wilson S A and Traynor R M 2015 Smart cement composites for durable and intelligent infrastructure *Procedia Eng.* **125** 796–803
[12] Saraireh D, Walls S, Suryanto B, Starrs G and McCarter W J 2017 The influence of multiple micro-cracking on the electrical impedance of an engineered cementitious composite *Proc. Int. Conf. on Strain-Hardening Cement-Based Composites* (Dordrecht: Springer) pp 292-9
[13] BSI 2019 *BS EN 197-1:2011: Cement – Part 1: Composition, specifications and conformity criteria for common cements* (London: British Standards Institution)
[14] JSCE 2008 *Recommendations for Design and Construction of High Performance Fiber Reinforced Cement Composites with Multiple Fine Cracks (HPFRCC)* (Tokyo: Japan Society of Civil Engineers)
[15] Suryanto B, Takaoka H, McCater W J, Saraireh D and Taha H 2018 Impedance measurements on an engineered cementitious composite: a critical evaluation of testing protocols *Measurement* **129** 445–56
[16] Suryanto B, Tambusay A and Suprobo P 2017 Crack mapping on shear-critical reinforced concrete beams using an open source digital image correlation software *Civ. Eng. Dimens.* **19** 2 93–8
[17] Tambusay A, Suryanto B and Suprobo P 2020 Digital image correlation for cement-based materials and structural concrete testing *Civ. Eng. Dimens.* **22** 1 6–12
[18] Suryanto B, McCarter W J, Starrs G and Chrisp T M 2017 Characterization of fly-ash using electrochemical impedance spectroscopy *Procedia Eng.* **171** 705–14
[19] Whittington H W, McCarter J and Forde M C 1981 The conduction of electricity through concrete *Mag. Concr. Res.* **33** 114 48–60
[20] Suryanto B, McCarter W J, Starrs G and Ludford-Jones G V 2016 Electrochemical immittance spectroscopy applied to a hybrid PVA/steel fiber engineered cementitious composite *Mater. Des.* **105** 179–89
[21] McCarter W J 1995 Effects of temperature on conduction and polarization in Portland cement mortar *J. Am. Ceram. Soc.* **78** 2 411–5
[22] McCarter W J, Starrs G and Chrisp T M 2000 Electrical conductivity, diffusion, and permeability of Portland cement-based mortars *Cem. Concr. Res.* **30** 9 1395–400
[23] Chrisp T M, Starrs G, McCarter W J, Rouchotas E and Blewett J 2001 Temperature-conductivity relationships for concrete: an activation energy approach *J. Mater. Sci. Lett.* **20** 12 1085–7
[24] Suryanto B, McCarter W J, Starrs G and Jablonski M 2017 Assessing the performance of engineered cementitious composites under cyclic wetting and drying *Proc. Int. Conf. on Strain-Hardening Cement-Based Composites* (Dordrecht: Springer) pp 573-81